Research on Engineering Structures & Materials
www.jresm.org
MIM Research Group

Research Article

Performance assessment of sustainable one-part alkali-activated concrete: An experimental and machine learning approach

Sujeet Kumar [*,a], Ajay Kumar Sinha [b]

Department of Civil Engineering, National Institute of Technology, Patna, 800005, India

Article Info

Article History:

Received 24 Feb 2026

Accepted 16 Mar 2026

Keywords:

One-part alkali-activated concrete;
Workability;
Strength;
Machine learning prediction;
Sustainability

Abstract

One-part alkali-activated concrete (OPAAC) is regarded as a sustainable substitute for traditional concrete and demonstrates significant potential in practical field constructions. This paper explores the properties of OPAAC made using a binder system that consists of ground granulated blast furnace slag, sodium metasilicate (SMS), and calcium hydroxide. Three mix designs for grades M15, M20, and M25 were formulated. The performance evaluations revealed that higher SMS content and water-to-binder ratio favored the workability of mixes. The hardened-state tests suggested that OPAAC showed an enhancement in compressive strength (CS), flexural strength (FS), and split-tensile strength (STS) with an increase in SMS content. The highest CS, FS, and STS recorded were 32.72, 6.20, and 3.44 MPa, respectively. Various machine-learning models were tested to estimate the strength of developed concrete. The gradient boosting model showed the best performance among others with an average test R^2 of 0.9684 and was able to successfully predict the strength. OPAAC also exhibited crucial environmental and economic advantages, including carbon reduction by 55-59% and cost savings by 12-16% compared to conventional concrete. Therefore, the outcomes show that OPAAC does not only present a comparable material performance but also an eco-friendly and less expensive option for the field construction activities.

1. Introduction

In the construction sector, concrete is the most utilized construction material on the earth, second only to water. This is mainly because of its abundance, affordability, and resilient nature. It is estimated that the annual production of concrete may rise from current 14 billion m^3 to 20 billion m^3 by 2050 [1]. But due to its dependency on traditional cement, there are serious environmental issues. Cement manufacturing is a very energy-consuming process that accords to about 8% of total man-made CO_2 emissions in the world with an amount of emission close to 0.80-0.95 kg of CO_2–equivalent per kilogram of ordinary Portland cement (OPC) [2]. In order to reach net-zero emission targets, the industry is increasingly using blended cements, such as Portland slag cement, Portland pozzolana cement, and composite cement. Composite cement (CC) is a more sustainable variant of blended cement with 23-47 % lower carbon emissions and it is largely used in various construction applications in Indian construction industry [3]. This has been largely due to the higher level of ground granulated blast furnace slag (GGBS) and fly ash (FA) and reduced content of clinker of 35-65 % [4]. In spite of the current developments, OPC continues to be a major contributor to carbon emission, thus explaining the need to focus on other binders that possess the latent to decrease carbon emissions and reduce the energy requirements. At the same time, the alternative binders should be locally available and economical with comparable strength and durability. Over the past decades, alkali-activated binders (AABs) were identified to be more sustainable substitute of the

*Corresponding author: sujeetk.ph21.ce@nitp.ac.in
[a]orcid.org/0000-0002-9875-2248; [b]orcid.org/0000-0002-2265-3008;
DOI: http://dx.doi.org/10.17515/resm2026-1531ma0224rs

conventional OPC. AABs utilize the industrial wastes such as FA, GGBS or metakaolin, as alumina-silicate precursors. These precursors are triggered by alkaline solutions (referred to as two-part AABs), which leads to the generation of stable alumina-silicate gels that act as a binding agent for aggregates and provide concrete with the normal strength properties. Traditional two-part AABs have already proved to have huge reductions in embodied carbon and their life-cycle analysis shows that they emit 40-80 % less CO_2 than OPC [5,6]. These values are mainly due to the avoidance of clinker and the use of industrial by-products. Apart from the enormous reductions in emissions, they happened to possess excellent mechanical properties and longevity compared to OPC [7,8]. Though two-part AABs are slowly gaining acceptance and several countries have already developed standards for their usage. Their application is currently hampered by the necessity to manage concentrated activator liquids, which is a safety, storage, and quality control issue on site [9]. To overcome the above concerns, one-part alkali activated binders (one-part AABs), also referred as "just-add-water" materials, have recently been developed [10]. These binders offer the sustainability and durability benefits associated with conventional AABs, while at the same time offering handling and placement similar to OPC. Recent researches have demonstrated that the concrete made using one-part AAB has excellent performances, which are high mechanical strength and greater durability in chemically hostile circumstances [11–13].

One-part alkali-activated concrete (OPAAC) renders as an eco-friendly and a practical substitute to traditional concrete. Simultaneously, OPAAC mitigates the challenges of managing corrosive liquid activators needed by two-part alkali-activated concrete and provides a better mechanical property and durability. The only difference that exists between OPAAC and traditional concrete is the composition of the binder. OPAAC requires a binder that composes a solid alumina-silicate materials and powder alkaline activators [14–16]. In production of OPAAC, GGBS is considered a highly reactive precursor because of its enhanced reactivity and amorphous structure. Due to their high CaO, SiO_2, and Al_2O_3 content, the formation of rigid and stable gel structures, majorly in form of calcium alumina silicate hydrate (C-A-S-H) gels occur, that results in high strength at early ages, good prolonged mechanical performance, and high durability [17–19]. But, higher content of GGBS in binder system reduces the workability of OPAAC [20] and, hence, it recommended to use the optimum GGBS content in the mix design of OPAACs. Overall, these superior properties of GGBS make it an excellent material to work within one-part systems [19,21]. On the other hand, sodium metasilicate (SMS) in forms of Na_2SiO_3-Anhydrous, $Na_2SiO_3.5H_2O$ and $Na_2SiO_3.9H_2O$, has been widely used as solid activators because of their high alkalinity and cementitious properties. Ma et al. [22] investigated the suitability of all threes forms of sodium metasilicate in one-part alkali-activated systems. They reported that Na_2SiO_3-Anhydrous has found to be best suited for the enhanced properties of one-part alkali-activated systems. But the usage of metasilicate may speed up the setting leading to efflorescence and cracking and result in lowering mechanical performances when overused beyond 14% of mass of binder system [11,17]. A body of research has indicated that, these problems can be alleviated by addition of supplementary solid activators like $Ca(OH)_2$, Na_2CO_3, NaOH or $NaAlO_2$ which help to improve the properties of binders as well as reduce early-age cracking [23–26].

Depending on the mix design, precursor type, activator ratio, and water-to-binder (w/b) ratio, OPAAC typically has a low workability, which requires more compaction efforts similar to conventional approach. It has been shown that the alteration of mix proportion, precursor type, activator ratio and w/b ratio affect the workability of one-part alkali-activated systems [20,27,28]. In same vein, the usage of traditional super-plasticizers improves the workability without affecting mechanical strength [25,29]. Haruna et al. [30] investigated the performance of OPAAC using a binder made of high calcium FA and solid Na_2SiO_3-Anhydrous. They reported that the workability of OPAAC was obtained in the acceptable range of 34–165 mm. An increase in paste-aggregate ratio resulted in a significant improvement in workability. In a recent study [31], the slump values for GGBS-based OPAAC, activated using SMS anhydrous, was reported in the range of 20–230 mm. This suggests that OPAAC with very low to high workability can be developed, which is useful for numerous structural applications from foundations to beam and slabs. The previous literature also indicates that OPAAC is capable of reaching a very high compressive strength (CS) as high as 70 MPa at 28-days of ambient or water curing, the flexural strength (FS) typically fell in the range of

4–7 MPa, and split tensile strength (STS) was in the span of 2–5 MPa at 28 d under similar curing methods [30,32–34]. These strength developments in OPAAC were mainly attributed to the occurrence of compact microstructure containing C-A-S-H gels as a major strength giving phase [17–19,26]. Nevertheless, the major influence on the strength was found to be due to mix formulation, precursor type, activator type, ratio of activators and w/b ratio, and the method of curing [9,15,16]. Research indicates that OPAAC is curable in both ambient and water. Water curing proved to be better in long term retention of strength and in providing better durability in case of OPAAC. This can be ascribed to the phenomenon that the water curing keeps the paste saturated in concrete matrix, which enhances ion diffusion and allows hydration reactions to persist at the interface of the paste and aggregates [18,30]. Furthermore, OPAAC has been found to have better durability compared to traditional concrete, with greater resistance to chemical attack, lower permeability, lower water absorption, and improved long-term performance, as suggested by previous studies [8,35,36].

In previous studies [37–42], the application of machine learning (ML) methods in the field of alkali-activated materials has become a common practice, primarily, to predict CS, identify effective influencing factors, optimize the mix proportions, and guarantee the quality control of mix. In literature review, it is implied that many ML models, including but not restricted to random forest, gradient boost, decision trees, support vector regression, ridge regression, lasso regression, ElasticNet, and artificial neural network (ANN) have been utilized to achieve the above-said. In a recent study [42], ML algorithms, including ANN and support vector machines, were studied on 3D-printed soil-cement composites. The authors also identified the necessity of standard datasets in order to overcome data scarcity and to enhance the reliability of the models. They suggested future research on the development of hybrid ML with physics-based simulations and exploration of environmentally friendly binders, including that these would be able to optimize local resources, improve longevity, and cut down emissions and expenses. Another study [43] has surveyed how digital twins and artificial intelligence (AI) can be used in real-time structural monitoring. These methods make it possible to monitor and identify anomalies earlier, and they turned out to be much more effective than the traditional approaches. Collectively, these studies demonstrate that there is a high potential of ML and AI in the material assessment, quality inspection, and structural health assessment. Nevertheless, the largest figure of studies on ML models was carried out on two-part AABs [37–40]. This makes use of ML models in OPAAC a less exploited area. Harika et al. [44] used five models of ML to estimate the CS of one-part AAB mortars. They train, test and validate the ML models using 135 experimental data. Findings indicated that the random forest model was the most predictive, with gradient boost and decision tree coming next, and support vector regression was the least predictive. In addition, they indicated that the content of the GGBS, activator dosage, curing age, and w/b ratio were the most affecting characteristics. In another study [45], application of models such as ANN and gene expression programming (GEP) in the prediction of OPAAC systems was presented using 171 experiments database. They added that ANN performed better as compared to GEP with regard to prediction efficacy. A sensitivity analysis indicated that the CS would be most affected by the activator and slag contents.

1.1. Research Significance

Although there is an increasing trend towards OPAAC, research in this area is still limited, and most of the research work has been carried out at the paste or mortar level, and not at the concrete level. There exists a gap in knowledge about selection and dosage of solid activators, mix design methods, fresh and hardened properties at concrete level or the application of ML methods in OPAAC. The current research aims to fill these gaps by assessing OPAACs in the M15 to M25 strength grades, which are widely utilized in practice, under different binder ratios and different levels of activators. Chemical activators of industrial grade were used for widespread applicability of binder systems. The proportions of mixes were designed in line with Indian standard mix design method. Such that one-part AABs could be equated with OPC and thus there was no need to develop new mix guidelines. The binders were pre-mixed and packaged for testing in a way similar to regular cement, which makes them easy to handle. Well-established testing methods were followed to determine the fresh and hardened concrete properties. Furthermore, ML models were applied for simultaneous predictions of the CS, FS and STS, which will enable fast formulation of mix

proportions, and guarantee quality control. Additionally, embodied carbon, and cost-effectiveness of OPAAC were assessed and compared with regular concrete. The current study provides detailed information about the application of OPAAC as a sustainable, economical, and practically feasible alternative to conventional concrete.

2. Materials and Methods

2.1. Materials

2.1.1. Solid Precursor and Activators

GGBS was employed as the alumino-silicate precursor in this research. Sodium metasilicate anhydrous (SMS) and calcium hydroxide (CH) mixture was employed as the solid alkaline activator. GGBS was procured form Astrra Chemicals, Chennai, India. Its chemical content was found through X-ray fluorescence (XRF) analysis, which showed that the mineral is predominantly made up of calcium with CaO constituting 42.7 % of the total oxide deposits as shown in Table 1. SMS, in granular form and of industrial grade, was obtained from Akshar Chem Exim Co. Pvt Ltd, Kolkata, India, and the supplier's specifications are listed in Table 1. CH, which was also purchased by the same supplier, was delivered as a fine industrial-grade powder with 96% purity of $Ca(OH)_2$. The use of industrial-grade activators in this study aimed at enhancing the applicability and feasibility of the proposed binder system. Table 2 shows physical characteristics of precursor and activators. Additionally, the particle size distribution curve of GGBS and activators are presented in Figure 1. As can be noted, SMS was significantly coarser than CH and GGBS. Further, the fineness of CH was higher than that of GGBS.

Table 1. Chemical compositions of GGBS and SMS

Constituents	CaO	SiO_2	Al_2O_3	MgO	MnO	SO_3	Fe_2O_3	Na_2O	LOI
GGBS (%)	42.7	31.2	15.1	5.71	1.63	1.19	0.68	-	0.26
SMS (%)	-	≥48	-	-	-	-	-	50-52	-

Table 2. Physical properties of GGBS, SMS, and CH

Descriptions	Specific Gravity	Blaine fineness (m^2/kg)	Mean particle size (μm)
GGBS	2.85	420	13.85
SMS	1.05	151	575
CH	2.21	450	11.75

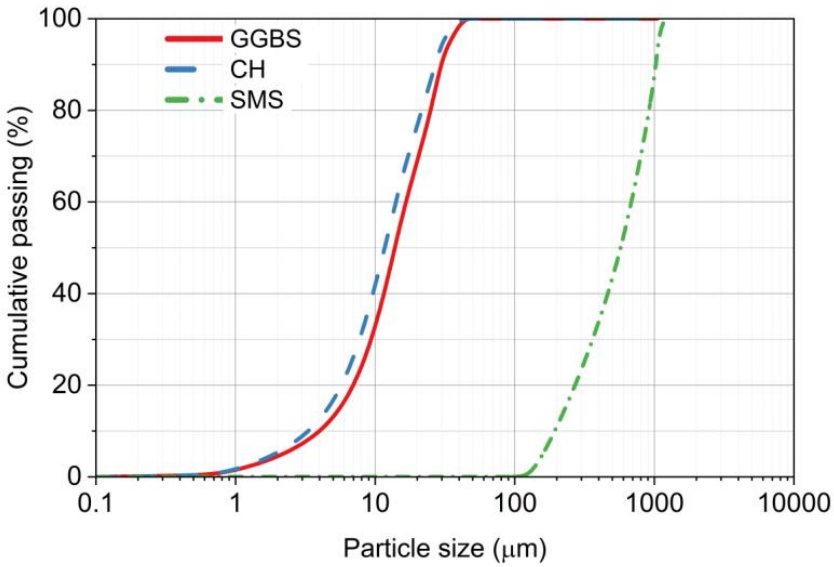

Fig. 1. Particle size distribution curves for GGBS, SMS, and CH

2.1.2. Binders

The current paper analyzed two different, one-part alkali-activated binders (AABs) designed to be used in concrete, with the content of each being 80% GGBS and 20% blended solid activators (SMS and CH). The first binder (AAB -1) had 14 % SMS and 6 % CH, and the second binder (AAB -2) had 12 % SMS and 8 % CH, the GGBS content was kept constant in both formulations. These ratios were fixed based on prior studies [17,26] and preliminary laboratory trials. For comparison purposes, a composite cement (CC) meeting the requirements of IS 16415:2015 [4] was also used. The CC, which is equivalent to 33-grade OPC, is a variant of blended cement made up of OPC, FA, and GGBS. According to the suppler' specification, CC was made up of 32.50% FA, 30.25% GGBS, and 37.25% OPC clinker, but excluding gypsum. The reasons for choosing the binder compositions, as well as the experimental work and performance assessment of the raw materials and binders, have been documented in the authors' previous work [46]. The binder properties are presented in Table 3. The performance analysis revealed that the physical properties of all binders were similar to those of 33-grade OPC and, hence, they were utilized in the design of concrete mixes.

Table 3. Physical properties of binders used in preparation of concrete mixes

Parameters	CC	AAB-1	AAB-2
Fineness (m^2/kg)	348±2	351±5	358±4
Specific gravity	2.84±0.04	2.64±0.02	2.58±0.02
Standard consistency (%)	32	29	32
Initial setting time (minutes)	134±6	55±5	76±2
Final setting time (minutes)	288±8	285±6	328±7
Soundness (mm)	1.2±0.1	2.0±0.2	1.8±0.3
Compressive strength (MPa), 28d	38.52±0.5	40.00±1.1	35.12±1.2

2.1.3. Aggregate and Water

The natural fine aggregate (NFA) used was local river sand, which conformed to Zone-III based on IS 383:2016 [47]. The nominal sizes of 20 mm and 10 mm of the natural coarse aggregates (NCA) were combined in a ratio of 60:40 based on laboratory trials to make a well-graded coarse aggregate of 20 mm nominal size, confirming to IS 383:2016 [47]. The physical attributes of NFA and NCA used in this study are provided in Table 4. Potable water that meets the criteria set out in IS 456:2000 [48] was used to produce all test specimens.

Table 4. Physical characteristics of fine and coarse aggregate

Descriptions		Fine aggregate	Coarse aggregate
Sieve Analysis	Size (mm)	% Passing	% Passing
	40	-	100
	20	-	90.5
	10	100	33.4
	4.75	100	0
	2.36	90.8	-
	1.18	76.2	-
	0.60	62.3	-
	0.30	15.2	-
	0.15	0	-
Nominal maximum size (mm)		4.75	20
Grading & Zoning		Zone-III	Graded aggregate
Specific gravity		2.64±0.01	2.80±0.02
Water absorption (%)		1.00	0.50
Compacted bulk density (kg/m^3)		1621±18	1606±22
Fineness modulus		2.56	6.76

2.2. Mix Proportioning and Sample Preparation

The mixes were formulated to produce three different grades of concrete (M15, M20, and M25), commonly used for residential buildings and general construction purposes, as per IS 10262:2019 [49]. The mixes were designed without using any chemical admixture. Thus, a low workability of concrete mix, target with slump value up to 50 mm, was selected during the mix design. During mix proportioning, the target CS (f'_{ck}) at 28 d for M15, M20 and M25 grades were adopted as 20.775, 26.60, and 31.60 MPa, respectively. It was set higher than the minimum characteristics CS (f_{ck}) of concrete as per the codal provision. Concrete mixes of each strength grade were produced using three different binders- AAB-1, AAB-2, and CC. The same proportions of ingredients and water-to-binder (w/b) ratios designed for AAB-1 binder were maintained across all the other binders of the same strength grade. All the concrete mixtures showed the intended workability, having slump values of 20–55 mm, during the laboratory trials. The common mixture ratios (binder: NFA: NCA) and w/b ratios were the following: M15- 1:1.85:3.64 (w/b = 0.55), M20- 1:1.58:3.07 (w/b = 0.48), and M25- 1:1.40:2.78 (w/b = 0.44). Table 5 shows the proportions of mixes in detail. Within the nomenclature, CC, A1 and A2 represent composite cement, AAB-1 and AAB-2 respectively, with the last two figures representing the grade of concrete strength.

Table 5. Mix proportions of different concrete mixtures used in the study

Mix ID	GGBS (kg/m³)	SMS (kg/m³)	CH (kg/m³)	CC (kg/m³)	NFA (kg/m³)	NCA (kg/m³)	Water (kg/m³)	W/B ratio
CC15	-	-	-	338.18	625.62	1230.30	186	0.55
A115	270.54	47.35	20.29	-	625.62	1230.30	186	0.55
A215	270.54	40.58	27.06	-	625.62	1230.30	186	0.55
CC20	-	-	-	387.50	614.01	1188.40	186	0.48
A120	310.00	54.25	23.25	-	614.01	1188.40	186	0.48
A220	310.00	46.50	31.00	-	614.01	1188.40	186	0.48
CC25	-	-	-	422.72	591.66	1175.70	186	0.44
A125	338.18	59.18	25.36	-	591.66	1175.70	186	0.44
A225	338.18	50.73	33.81	-	591.66	1175.70	186	0.44

Fig. 2. Freshly prepared concrete mixture, the slump cone test, and prepared test specimens

The concrete was made by first dry mixing the required quantities of binder, NFA, and NCA for 2 min in a laboratory pan mixing machine. After this, the measured quantity of water was added as per the prescribed w/b ratio as mentioned earlier. The mixing was performed for further 3-5 min till the mixture attained a homogeneous consistency. All the mixing and casting were done in a laboratory setting, which was maintained in range of 27 ± 2 °C temperature and 65 ± 5% relative humidity. The concreting process was followed same as the standard procedure generally adopted for conventional concrete. Figure 2 shows the freshly prepared mixture, the slump test on the fresh mix, and the prepared cubic, cylindrical, and prismatic moulds. Concrete was immediately poured into different moulds: cubic moulds of 150 x 150 x 150 mm, cylindrical moulds of 150 mm diameter x 300 mm height, and prismatic moulds of 500 x 100 x 100 mm. A table vibrator was used to compact each mould for removing entrained air and achieving dense specimens. The compacted mould was, then, covered with wet cloths and left in a laboratory atmosphere for a period of 24±2 h prior to demolding. After demolding, the test samples were submerged in a temperature-controlled curing tank, which was regulated at 27 ± 2 °C. The samples were cured in the curing tank until the time of test.

2.3. Experimental Methods

2.3.1. Test On Fresh and Hardened Properties

The workability of the prepared mixtures was measured using the slump test according to the IS 1199 (Part 2): 2018 [50]. For slump cone test, a common reference mixes with (binder: NFA: NCA) ratio of 1:1.40:2.78, referring M25 grade mix, was selected in order to explore the influence of w/b ratio on the workability. The w/b ratio was altered stepwise (0.40 to 0.60) and the slump tests were conducted on each of the w/b ratios to establish the effects of the water content in the fresh concrete mixture on the workability. For every mix and w/b ratio, three slump tests were performed, and the average slump value was recorded and reported.

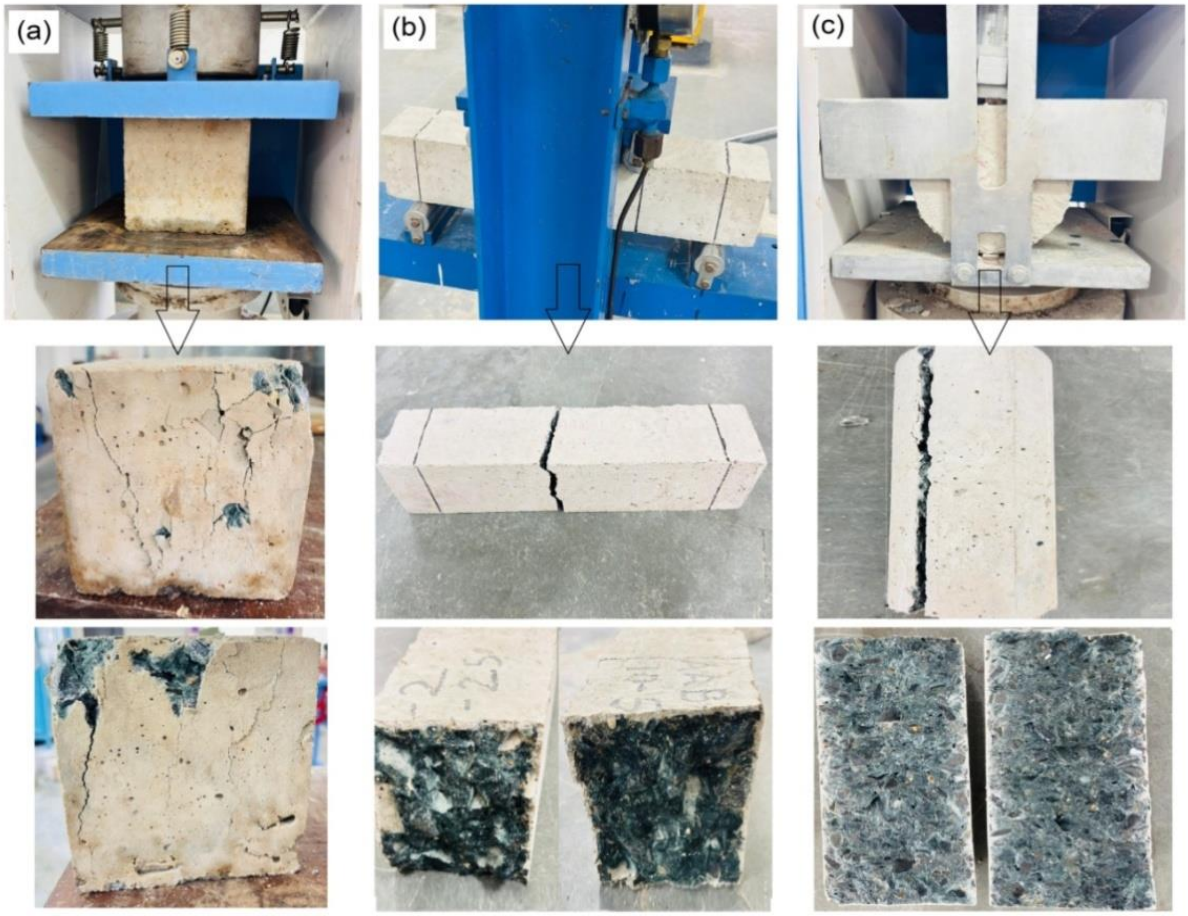

Fig. 3.Test set-up and failure mechanisms of concrete specimens

The CS, FS and STS tests were conducted to identify the mechanical properties of hardened OPAAC as per the methodology suggested in IS 516 (Part 1/Sec 1): 2021 [51]. All experiments were also carried out in a laboratory environment at 27 ± 2 °C temperature and 65 ± 5% relative humidity. Specimens were tested after 3, 7, and 28 d of water curing to determine the development of strength with time. CS and STS of all specimens were obtained through a digital compression test machine with the associated accessories, and FS was obtained on prismatic specimens through a four-point flexural set-up using a flexural testing machine. The test set-up and failure mechanism of the specimens were akin to that of traditional concrete as shown in Figure 3. Three replicate specimens were tested at every curing period with each mix proportion and mean values were recorded. A total of 81 cube specimens were subjected to CS tests, 81 prismatic beam specimens to FS tests, and 81 cylindrical specimens to STS tests, putting into consideration all mix proportions and the curing periods.

2.4. Machine Learning Methodology

The present modeling study was performed on the basis of the experimental strength results, which were conducted on 09 different mixes of concrete (Table 5). Parameters recorded include CS, FS and STS at the curing age of 3, 7, and 28 d. There were 81 specimens that were tested, inclusive of all curing ages, in each strength test. Therefore, 81 data point featuring 08 input variables (GGBS, SMS, CH, CC, NFA, NCA, w/b ratio, and curing time) and 03 output variables (CS, FS, STS) were prepared for modeling study. Table 6 shows the input (feature) and output (target) variables that were utilized in the modeling with their specifications. Preprocessing of the experimental data was done before modeling to eliminate possible inconsistencies. The data were preprocessed followed by the division of the data into eight input features and three output targets. In order to achieve an objective evaluation of model performance, the data were randomly divided into two sets- 80% training set for model development and 20% testing set for evaluation.

Table 6. Dataset properties of input and output variables

Parameter	Minimum	Mode	Median	Mean	Maximum	Standard deviation
GGBS (kg/m^3)	0	0	270.54	204.16	338.18	147.04
SMS (kg/m^3)	0	0	46.5	33.18	59.18	24.1
CH (kg/m^3)	0	0	23.25	17.86	33.81	13.25
CC (kg/m^3)	0	0	0	127.6	422.72	182.69
NFA (kg/m^3)	591.66	625.62	614.01	610.43	625.62	14.18
NCA (kg/m^3)	1175.7	1230.3	1188.4	1198.13	1230.3	23.47
W/B ratio	0.44	0.55	0.48	0.49	0.55	0.05
Curing time (days)	3	3	7	12.67	28	11.03
CS (MPa)	8.67	10.6	18.2	19.12	34.2	6.7
FS (MPa)	1.01	2.98	3.22	3.27	6.5	1.37
STS (MPa)	0.7	0.79	1.82	1.85	3.62	0.76

Similar to prior studies in the field of ML application in the prediction of concrete properties [37–40,44,45], five supervised learning models were used: Ridge Regression (RR), ElasticNet (EN), Support Vector Regression using radial-basis-function kernel (SVR), Gradient Boosting (GB) and Random Forest (RF). Simultaneously, since the task involved predicting several output variables, multi-output regressor was employed to generalize single-output regressors to multi-target prediction. In algorithms that can make use of feature scaling (RR, EN, SVR), the input variables in a preprocessing pipeline were standardized with a Standard Scaler to provide an appropriate normalization. The model performance was measured through the "repeated K –fold cross-validation", where 5-folds were repeated twenty times to obtain a robust performance estimate. Evaluation metrics of the models were the "coefficient of determination (R^2)", "root-mean-square error (RMSE)" and the "mean absolute error (MAE)" [37]. After the procedure of cross-validation (CV), every model was again trained on the entire training set and then tested on the held-out test subset in order to have an unbiased estimate of the predictive generalization. An over-fitting score, which is the difference between the mean training R^2 and the mean CV R^2 was calculated to measure

generalization capacity and detect the possibility of over-fitting. In order to find the share of individual input variables to the strength predictions, feature-importance analysis was conducted on the best model. The best model was applied to hyperparameter optimization using GridSearchCV in order to find the best parameters of learning rate, tree depth, and the number of estimators. This was followed by the utilization of the Leave-One-Out Cross-Validation (LOOCV) of un-tuned and tuned versions of the top model on the complete dataset. This furnishes an additional evaluation of the generalization especially in the case of a small amount of data. The resulting optimized model was ultimately used to provide predictions of new input parameters demonstrating its practical use.

3. Results and Discussion

3.1. Workability

The workability of concrete mix contributes significantly to the abilities of the fresh mixture besides the strength and long-term properties of concrete. Figure 4 displays the slump values of all concrete mixes corresponding to different w/b ratio (0.40–0.60). The results show that the values of slump in all concrete mixes were in the range of 10–85 mm, categorized as very low to medium workability. AAB-1 concrete mixes outperform CC mixes as well as AAB-2 mixes in workability at each level of w/b ratio. The increase in w/b ratios enhanced the slump values by lowering the frictional forces between the particles and thereby, enhancing the flowability of the mix [29]. It is relevant to add that A125 mix had slightly higher slump values in comparison to control mix, CC25 and A225 concrete mix. This is due to greater SMS content (14%) and lower CH (6%) in binder composition of A125 concrete mix. The SMS/CH activator ratio is found to be directly related with the workability of OPAAC mixes. The lower silica modulus of SMS used (SiO_2/ Na_2O ~0.9) has helped in improving the workability by faster dissolution of SMS particles in the fresh state of OPAAC mixes [10]. In a previous work, Oderji et al. [20] investigated FA and GGBS- based OPAAC systems. They reported that SMS anhydrous provided higher flowability and enhance strength compared to other solid activators used. On the contrary, the increase in CH content tends to reduce the fresh workability of OPAAC, which may be attributed to the particle packing influence of finer particles of CH in fresh mixture [24]. These finding collectively suggests that OPAAC has similar performance to CC concrete in terms of workability.

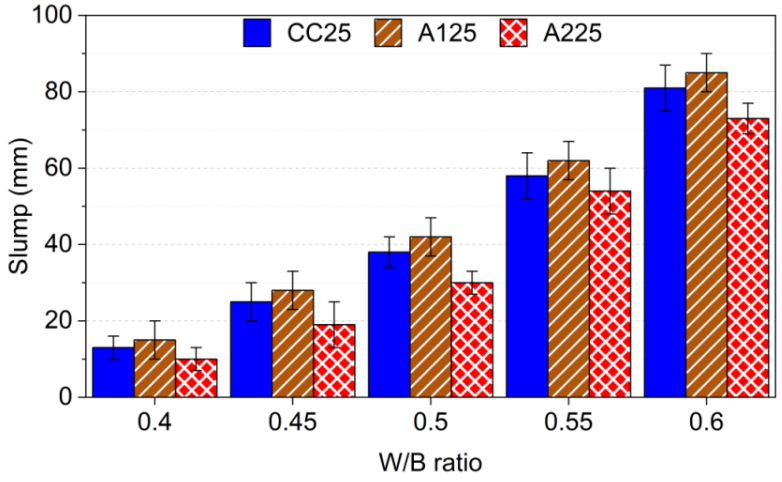

Fig. 4. Slump values of concrete mixes based on different w/b ratios

3.2. Mechanical Performances

3.2.1. Compressive Strength

The CS of concrete is the most essential characteristic on which the quality, effectiveness and adaptability of concrete mixes relies upon. Figure 5 illustrates the CS of all designed concrete mixtures, measured at 3, 7 and 28 d of curing ages. In all mixtures, the CS increased gradually with

age upon continuous hydration under water curing. In every concrete grades, the mixes, prepared using all three binders, exhibited CS well above f_{ck} values, meeting the minimum criteria. In AAB-1 and CC concretes, the mixes not only met but also surpassed f'_{ck} values in all the respective grades. But, AAB-2 concrete mixes had values that were close but fell short of f'_{ck} in all the grades. The SMS/CH activator ratio is found to be directly related with the CS of OPAAC. Higher the SMS content tends to enhance the strength development. AAB-1 concrete mixes always exhibited the highest CS at all the ages compared to both of CC and AAB-2 concretes. The highest CS value obtained for AAB-1 mixes in M15, M20 and M25 grades was 22.38, 27.88 and 32.72 MPa, respectively. The reason may be the higher SMS (14%) and lower CH content (6%) in binder composition of AAB-1. The elevated SMS content resulted in the rapid dissolution of GGBS and yields to the accelerated production of C-A-S-H gels, which are regarded to be the major strength-providing entities in GGBS-based OPAAC [17,18].

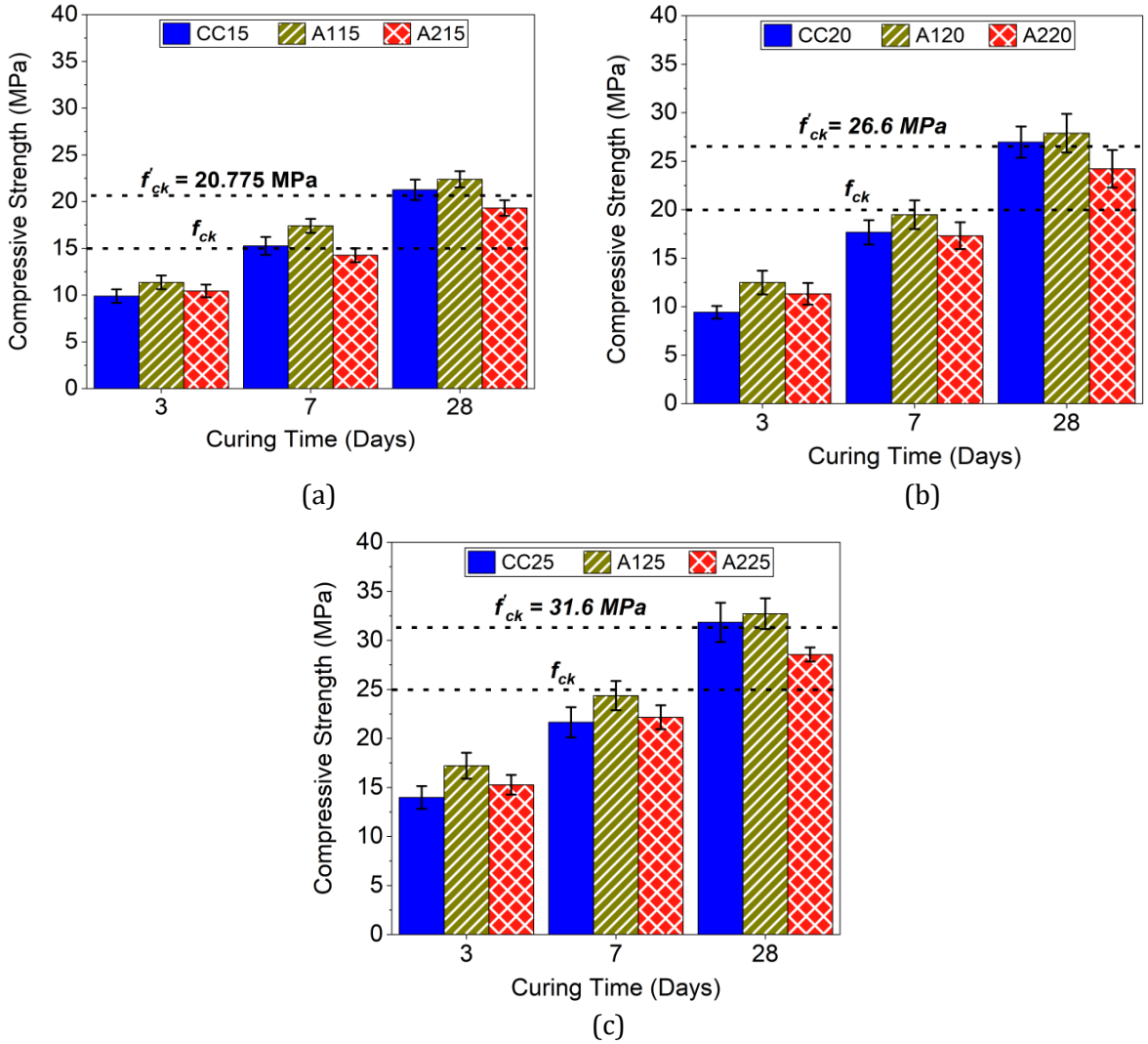

Fig. 5. Compressive strength of M15, M20 and M25 mixes

Additionally, the CH particles present in the binder also contributed to gel formation by making the calcium soluble and, thus, it reacts with the dissolved SiO_2 and Al_2O_3 to achieve a denser and more interconnected pore structure [24]. This did not only enhance the values of CS but also produced test specimens free from common defects such as efflorescence and cracking, as observed from their visual appearance (Figures 2f and 3), indicating improved matrix integrity. It is noticeable that SMS content plays the major influential role in strength developed and complemented by auxiliary activator CH to produced dense concrete products. The strength development rate of OPAAC at early age was more compared to CC concrete. CC concrete reached approximately 42 % and 68 % of its 28 d CS at 3 and 7 d, respectively, whereas OPAAC mixes reached approximately 50 % and 74 % of its 28 d CS, respectively. This is given the fact that despite being very reactive, GGBS

dissolves well with the alkali activators which are known to be catalysts in the initial development of C-A-S-H gels. In a similar research, Ma et al. [22] presented that GGBS-based OPAAC systems show a rapid development of strength at an initial curing age (3 and 7 d), and a decelerated strength development at a higher age (beyond 28 d). Overall, these findings show the potential of OPAAC to develop M15, M25 and M25 grades concrete, applicable to various concreting applications.

3.2.2. Flexural Strength

The FS of concrete is a basic mechanical characteristic utilized to determine its tensile resistance to rupture under flexural stresses. In case of normal concrete, the strength in tension is estimated by the relation between FS and CS that has been given in the IS-456:2000 code [41] as f_{cr} =0.7$\sqrt{f_{ck}}$. Figure 6 shows the FS of all prepared concretes at curing ages of 3, 7 and 28 d. Similarly, to CS, FS increased with time of curing, due to the ongoing hydration under water curing. All the concrete mixes had reached the desired FS values after 28 d, which is 2.71, 3.13, and 3.50 MPa with M15, M20 and M25 grades, respectively. The FS of AAB-1 concrete was the highest of the mixes, recording the highest values of FS at 4.02, 5.08 and 6.20 MPa for M15, M20 and M25 grades, respectively. These values of AAB-1 concrete were significantly higher than the f_{cr} value, probably as the result of the high-quality binder paste bonding behavior between the binder paste and the aggregates [30].

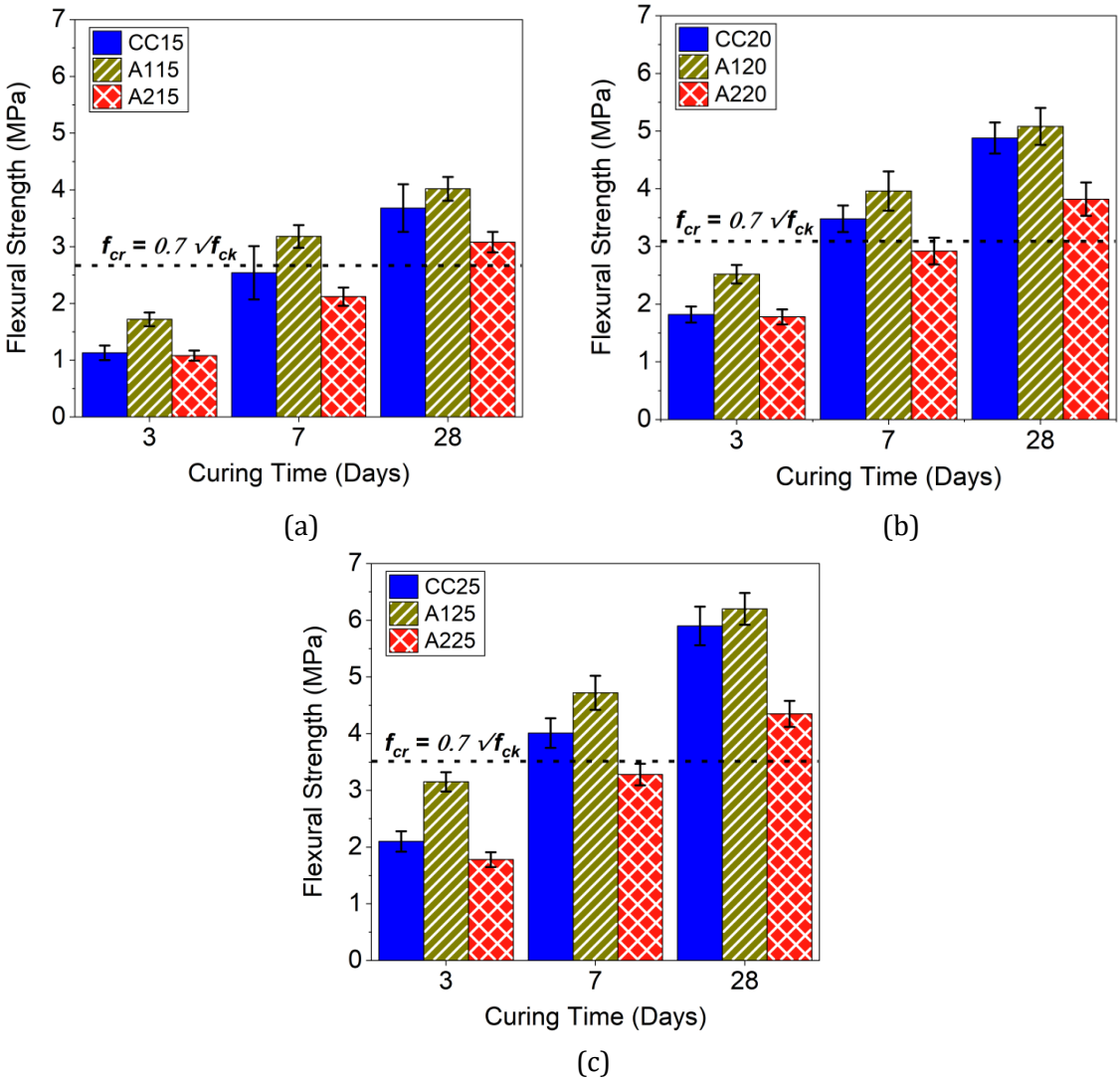

Fig. 6. Flexural strength of M15, M20 and M25 mixes

Figure 3b clearly shows the test specimen failure mode during flexural loading, which shows that the specimen is mostly intact after failure. The high FS values of AAB-1 concrete mixes can be explained by high SMS content (14 %) of the binder mixture composition which predisposes rapid

alkali-activation and creation of high density, interlocking C-A-S-H gels network [18]. Similar to behavior of CS, SMS content stands out as a leading influential factor that is moderated by CH content in the development of FS. When the SMS/CH ratio increases, FS is increased and when the ratio decreases the FS decreases. Lower FS values were observed using the reduced SMS content (12 %) in the AAB-2 concrete mixes than the CC and AAB-1 concretes. The FS/CS ratios at 28 days of curing were 0.17–0.18 in CC, 0.18-0.19 in AAB-1 and 0.15-0.16 in AAB-2 across all grades. These ratios are higher than the standard range of f_{cr} which is about 10-15% of f_{ck} and the FS values were more than that calculated by the relation f_{cr} =0.62$\sqrt{f_{ck}}$ as specified by ACI 318-05 [52]. Similar to standard concrete, the FS of OPAAC is directly proportional to its CS; the mixes with higher CS values achieve a higher FS and, conversely, as well. On the whole, flexural behavior of OPAAC shows its potential to be used in various construction applications like casting of beams, slabs, and pavements.

3.2.3. Split Tensile Strength

The STS is another vital parameter utilized to measure the direct tension capacity of concrete to withstand cracking. Figure 7 displays the STS of all prepared mixes at 3, 7 and 28 d of water curing. The STS was also a reflection of the overall trend of CS, where strength gained progressively as the curing continued. IS 456: 2000 code does not imply any definite relation to estimate STS, thus, the standard relation to estimate STS on 28 d, f_{ct} =0.56$\sqrt{f_{ck}}$, as suggested by ACI 318-05 [46], was used.

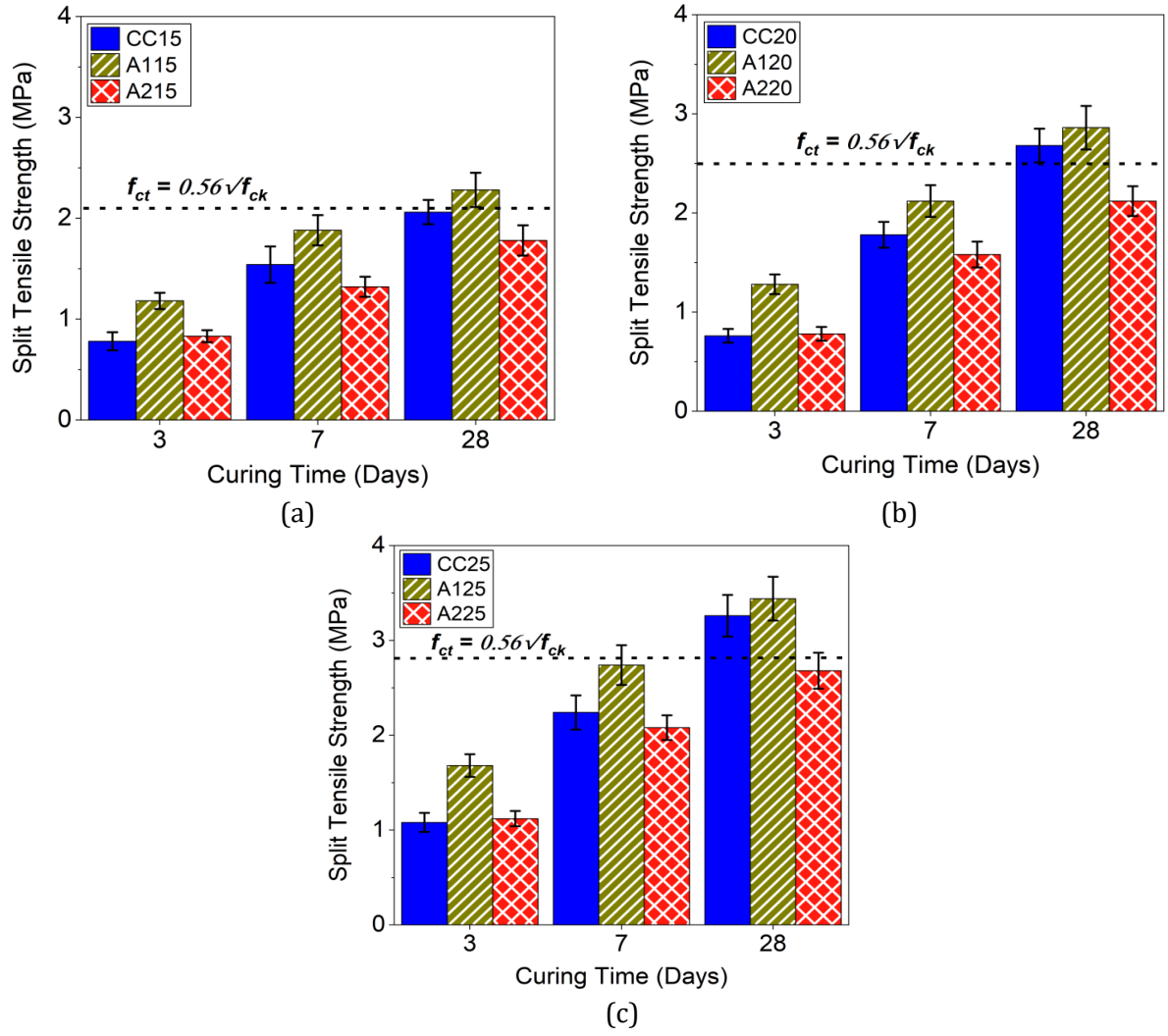

Fig. 7. Split tensile strength of M15, M20 and M25 mixes

These findings show that the AAB-1 and the CC concrete mixes meet the necessary f_{ct} of 2.17, 2.50, and 2.80 MPa at 28 d of water curing for M15, the M20 and the M25 grades, respectively. In AAB-2 concrete mixes, the observed f_{ct} values fall below the thresholds. However, they have STS values

above the general benchmark of 8 % of f_{ck} across all grades. AAB -1 concrete mixes recorded maximum STS values of 2.28, 2.86 and 3.44 MPa at the M15, M20 and M25 grades. The higher values were observed in OPAAC as a result of the good bonding behavior between the binder paste and aggregates [30]. As seen in Figure 3c, failure mode of the split tensile test could be very clear and shows that even upon failure; the specimen is left relatively intact.

In line with the behaviors of CS and FS, the high STS values of AAB-1 concrete mixes may be explained by the high level of the SMS content (14%) in its binder composition that facilitates the rapid alkali-activation and occurrence of a dense and interlocked C-A-S-H gels network [18,31]. Similar to CS and FS, SMS content is a decisive factor that is moderated by CH content in the development of STS. Increasing the SMS/CH ratio increases STS and a decrease result in lower STS values; to this end, the lower SMS content of AAB-2 concrete mixes (12%), provided lower STS values compared to CC and AAB-1 concrete mixes. The ratio of STS/CS between 28 d of curing among all grades was 0.09 -0.10 in CC, 0.10-0.11 in AAB-1, and 0.08-0.09 in AAB-2. Simultaneously with the traditional concrete, STS of OPAAC is directly proportional to its CS; higher CS values of mixes yield higher STS and vice versa. In sum, STS performance of OPAAC is evidenced to have superior resistance to cracking when subjected to tensile stresses, therefore making it a suitable choice for the concrete structures.

3.3. Machine Learning Based Strength Prediction

A comprehensive ML framework was used to forecast multiple concrete strength variables simultaneously. Such that, a single model could be used to analyze CS, FS, and STS with respect to material compositions and curing conditions.

3.3.1. Feature and Target Correlations

Figure 8 presents the feature and target correlation heatmap. In feature-feature correlation, the heatmap shows a number of strongly significant positive and negative relationships between the input features. GGBS, SMS and CH (Ingredients for one-part AAB) have high positive correlations with each other (0.93 to 0.99) and negative correlations with CC (-0.95 to -0.98). This observation shows that there is a purposeful mechanism of substitution that is between the two systems of binders. Independent variation is observed when the one-part AAB (made of GGBS, SMS, and CH) is used in place of CC. Such strong relationships are expected to occur in mixture designs where two systems of binder compete with fixed total binder content, and this poses inherent interdependence of compositions [41]. Similarly, there is a strong inter-correlation of NFA and NCA, and the correlations of these variables to the w/b ratio (0.89 to 0.99) are also high, which shows that aggregate and water content correlate with each other to maintain concrete properties. Curing time is showing no relation with the material compositions, as it is an independent variable rather a compositional variable. To tackle such complex correlations between features, five different models were used in this research for the prediction the strength of concrete.

In feature to target correlation, curing time has the greatest positive influence on CS (0.79), STS (0.74), and FS (0.73), as indicated in the feature-target correlation matrix, thus proving that long curing periods have a significant positive impact. The aggregates and w/b ratio have moderate negative relationships (-0.36 to -0.46), which means that their ratios should be well balanced to produce the best strength. GGBS, SMS and CH (making up the one-part AAB) and CC exhibit lesser lineal correlations, indicating that their roles may rely on nonlinear or synergistic interactions among the binder system components, but participate in a main role in the all-round performance of the materials.

3.3.2. Model Comparison

The relative performances of the five ML models show distinct differences in prediction capability of multi-output strength. Table 7 presents the comparative results of RR, EN, SVR, RF, and GB on the training, validation, and testing data using the R^2, RMSE, and MAE as the evaluation measures. The most accurate predictive models in the training dataset were those based on ensembles (RF and GB). GB achieved the highest training (R^2 score of 0.9797) and minimum RMSE (0.416 MPa) and MAE (0.3431 MPa) followed by RF (R^2=0.9739).

Fig. 8. Feature and target correlation heatmap

Table 7. Comparative results of models on training, validation and testing data

Model	Training data			Validation data			Testing data		
	R^2 Score	RMSE (MPa)	MAE (MPa)	R^2 Score	RMSE (MPa)	MAE (MPa)	R^2 Score	RMSE (MPa)	MAE (MPa)
RR	0.8259	1.1052	0.9269	0.7444	1.2145	1.0285	0.8386	1.5333	1.0437
EN	0.7671	1.1872	0.9821	0.6772	1.295	1.0811	0.7409	1.7018	1.1621
SVR	0.9300	0.8480	0.6415	0.8241	1.1778	0.9997	0.9176	1.4478	0.9145
RF	0.9739	0.4520	0.3742	0.9096	0.7618	0.6314	0.9560	0.8063	0.4764
GB	0.9797	0.4160	0.3431	0.9219	0.7326	0.6184	0.9675	0.7525	0.4360

The capability of good fitting was also shown by SVR (R^2 = 0.9300), but not the linear models RR (R^2 = 0.8259) and EN (R^2 = 0.7671). The high accuracy of GB and RF in training suggests the fact that both models have very strong ability to follow nonlinear trends in the dataset. The results of the validation indicate a weak deterioration in the performance of all models, as expected in the measurement of the generalization ability.

It was observed that GB had the best validation (R^2 = 0.9219) and minimum RMSE (0.7326 MPa) which demonstrated that the predictive performance remained stable and reliable across cross-validation folds. RF also exhibited good validation (R^2 = 0.9096). On the other hand, SVR had a greater decrease in the R^2 between training and validation (0.9300 to 0.8241) indicating a relatively high sensitivity to the variation of data. The linear models still showed inferior validation results with EN providing the poorest results (R^2 = 0.6772).

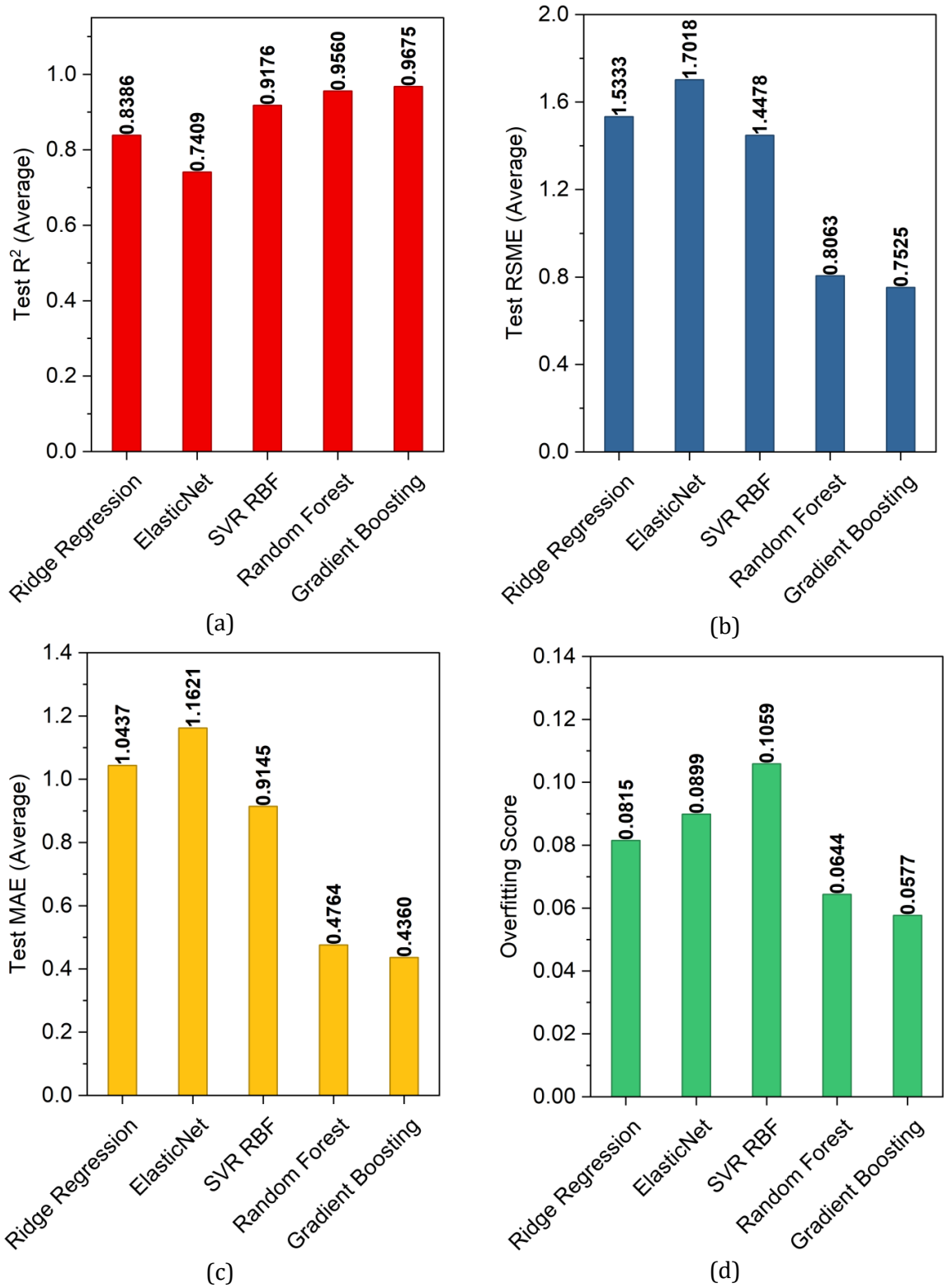

Fig. 9. Comparison of overall test performance across all models

The excellence of ensemble techniques is also supported by testing performance, as displayed in Figure 9. GB has the highest test R^2 of 0.9675 and the smallest RMSE of 0.7525 MPa and MAE of 0.436 MPa. Hence, it exhibits good predictive power and generalization. RF ranked close (R^2 = 0.9560) and SVR performed mediocrity (R^2 = 0.9176) with greater error measures. RR and EN showed relatively lower test accuracy as they have a small ability to represent complex nonlinear relations. Overfitting analysis further validated these results (Figure 9d). SVR showed the highest overfitting score of 0.1059, which reflects a larger gap between training and validation metrics. In contrast, GB showed the lowest overfitting value of 0.0577, suggesting balanced learning behavior

and effective generalization without excessive memorization of training data. In general, the outcomes show that ensemble ML methods, especially GB, are more effective in terms of predictive ability in all data partitions. The comparatively low gap between training, validation, and testing measurements of GB and RF suggests that the model complexity can be under control and the generalization of the model can be high, but the high-performance difference between SVR and the linear models suggest the relatively reduced robustness.

Table 8 presents the evaluation metrics of all the assessed models in terms of the test performance with regard to CS, FS and STS. In CS prediction, GB with R^2 = 0.9669 had the greatest predictive power with the lowest values of RMSE (1.2677 MPa) and MAE (1.0065 MPa). RF was also close behind (R^2 = 0.9627). The SVR demonstrated moderate results (R^2=.8742) in comparison with RR and EN that generated relatively lower accuracy and higher error rates. Ensemble methods were once again the best in the estimation of FS. The best R^2 of 0.9639 with the least error measures was achieved by GB and the second best R^2 of 0.9486 was by the RF. SVR also gave a very good performance (R^2 = 0.9362) which is much higher than that of the linear models. EN posted the lowest result of this target (R^2 = 0.6431). Similarly, in predicting STS, GB performed the best with (R^2 = 0.9715) followed by RF (R^2 of 0.9566) and SVR (R^2 of 0.9424). The linear models are also associated with relatively smaller values of R^2 and larger values of error. On the whole, the results show that ensemble methods, in particular, GB and RF, always have better predictive accuracy by all measures of individual strengths. Compared to linear models, SVR is still competitive in FS and STS, but it has a low capacity to model non-linear and complex relationship inherent to the features.

Table 8. Target-specific prediction accuracy of all models

Model	CS test			FS test			STS test		
	R^2 Score	RMSE (MPa)	MAE (MPa)	R^2 Score	RMSE (MPa)	MAE (MPa)	R^2 Score	RMSE (MPa)	MAE (MPa)
RR	0.8650	2.5603	2.2595	0.8063	0.3714	0.3231	0.8445	0.6006	0.5484
EN	0.8387	2.7989	2.4247	0.6431	0.5041	0.4070	0.7410	0.7752	0.6546
SVR	0.8742	2.4717	2.2608	0.9362	0.2131	0.1717	0.9424	0.3654	0.3111
RF	0.9627	1.3465	1.0556	0.9486	0.1913	0.1407	0.9566	0.3171	0.2330
GB	0.9669	1.2677	1.0065	0.9639	0.1602	0.1192	0.9715	0.2570	0.1824

3.3.3 Performance of The Best Model

The comparative analysis found GB to be the best model among others, and, hence, it was selected to be refined further. To improve its estimation accuracy, hyperparameter tuning was used and the findings are tabulated in Table 9. The predictive accuracy of the tuned GB model had a small increase in comparison with the original one. Test R^2 slightly rose to 0.9684 out of 0.9675, whereas RMSE fell to 0.7412 MPa out of 0.7525 MPa with MAE declining to 0.4353 MPa out of 0.4360 MPa. Moreover, the overfitting measure dropped to 0.0575 by a small margin compared to 0.0577, indicating a slight but significant increase in the level of generalization ability. Though the measured improvements are small, it is a pointer to the fact that the original model had already been highly optimized and stable.

GridSearchCV identified the optimal hyperparameters as estimator learning rate = 0.1, max tree depth = 3, number of estimators = 50 and the best CV Test R^2 score was 0.9222. The overfitting score of tuned GB model was the difference between CV train R^2 of 0.9797 and CV test R^2 of 0.9222. The optimization process was useful in minimizing prediction error and slightly improving robustness without a significant increase in overfitting. In turn, the tuned GB model gives the highly precise and reliable predictions on the estimation of strength.

In the final validation of model, LOOCV showed that tuned GB model had slightly better RMSE and MAE (0.5467 MPa vs 0.5473 MPa in both) compared to the untuned model. These minor enhancement in RMSE and MAE for the tuned GB model suggested that the tuning process indeed led to a more precise and generalizable model performance, even when tested with the most granular cross-validation process. The final model did very well for predicting various strength targets based on the provided material compositions and curing conditions.

Table 9. Hyperparameter tuning effect on gradient boosting model

Descriptions	Test R^2Score	Test RMSE (MPa)	Test MAE (MPa)	Overfitting Score
Untuned GB model	0.9675	0.7525	0.4360	0.0577
Tuned GB model	0.9684	0.7412	0.4353	0.0575
Change in metrics	+0.0009	-0.0113	-0.0007	-0.0002

Furthermore, the feature importance analysis of the best model is displayed in Figure 10. The importance of the feature analysis of the GB model indicated that curing time had the highest predictive power since it showed 69.16% of overall performance. This dominant significance implies that the target variable is very sensitive to the period of curing; this coincides with the established behavior of time-dependent strength development in concrete [30,39]. Out of the compositional parameters, SMS (8.23 %) and NCA (8.12 %) had significant contribution. The rest had a lower contribution, namely NFA (4.68 %), w/b ratio (4.51 %), and CH (4.11%). In contrast, CC (1.02 %) and GGBS (0.17%) indicate little influence due to nature of current mix compositions in the present modeling framework.

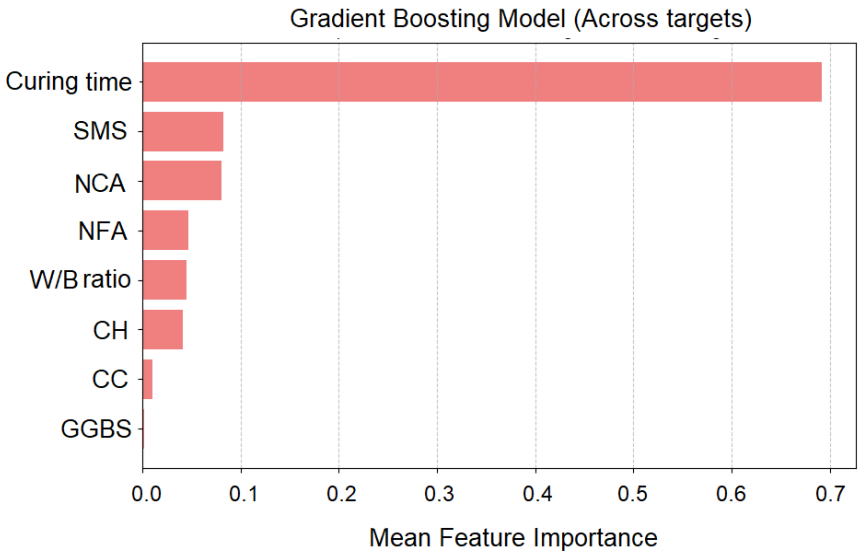

Fig. 10. Mean feature importance for the best model across all targets

Figure 11 present the actual vs predicted strength along with prediction errors of tuned GB model. The model showed excellent predictive power, with respect to all the three mechanical strength as indicated by high score of R^2. The tuned model had R^2 of 0.9679, 0.9716 and 0.9656 thereby explaining more than 96 percent of the variance in the experimental scores. FS was the most predictive of the three targets, followed closely by CS and STS, which verify the predictability of the model using the different mechanical responses. The strength of the model is also supported using the error analysis. On CS, the model yielded an RMSE of 1.2480 MPa and an MAE of 1.0072 MPa, which demonstrates a slight average deviation of the model generated and actual values in terms of an average strength range of the entire spectrum. In the case of FS, predictions produced RMSE of 0.2567 MPa and MAE of 0.1816 MPa. Similarly in STS, RMSE of 0.1566 MPa and MAE of 0.1172 MPa, which indicates a very accurate prediction with a very limited variation. which is equal to remarkably small absolute prediction errors.

The low and stable values of RMSE and MAE in all target variables and the high values of R^2 indicate that the model does not only capture the variance effectively but also maintains a good level of numerical accuracy. The strength of the model further is proven by a close analysis of the errors of predictions. In CS, most of the deviation lies in the range of about ±2 MPa even at high strength levels of over 30 MPa and this shows consistency in performance at both low and high strengths. The FS predictions are tend to exhibit low deviations of ±0.4 MPa, whereas the error on STS is about

±0.2 MPa. Even though some slight overestimations are noted at some higher levels of strength, the errors are symmetrically distributed and they do not indicate any systematic bias or instability.

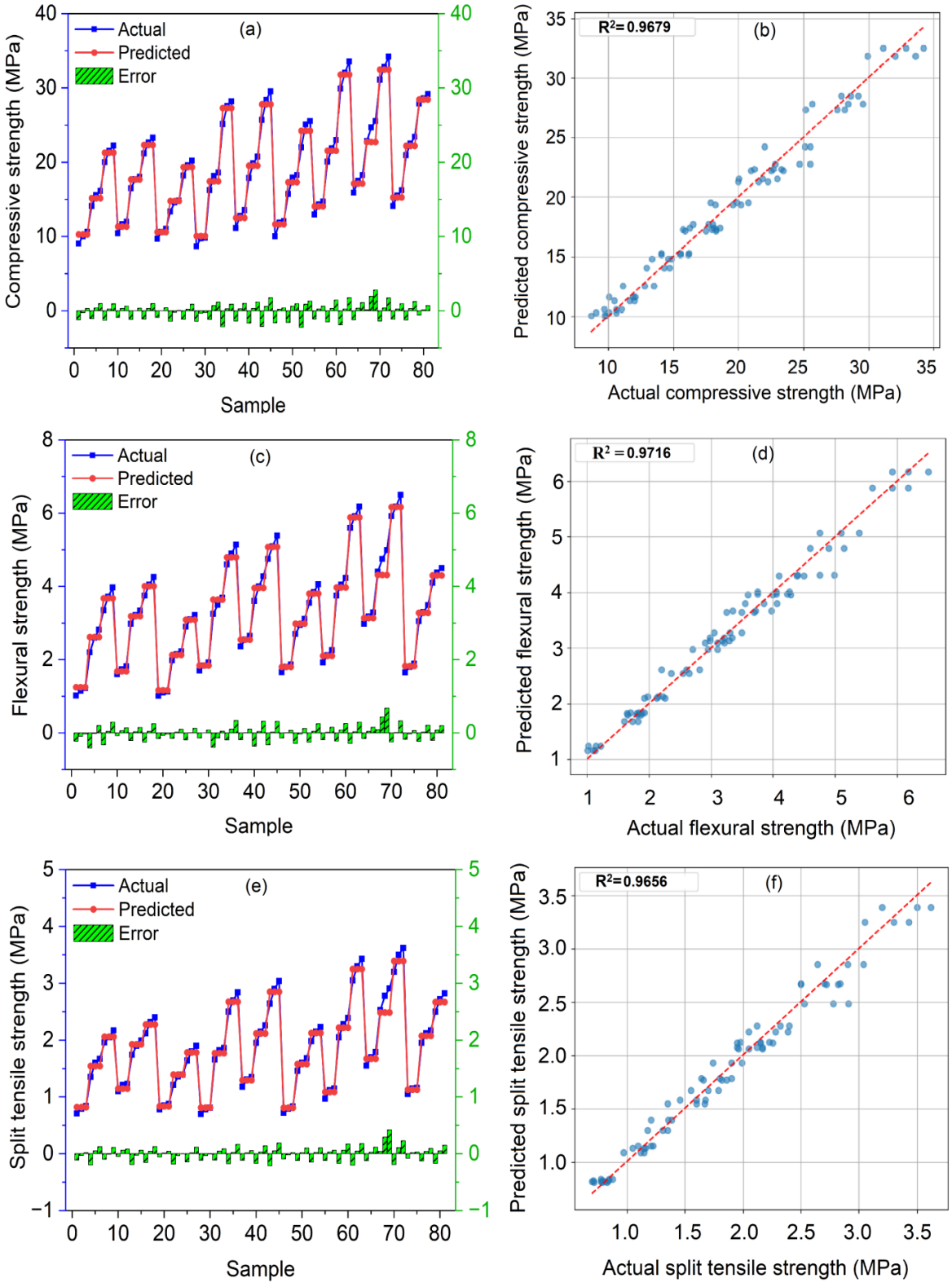

Fig. 11. Actual vs. predicted results of tuned gradient boosting model

Significantly, the model was also able to describe the internal relationship between the mechanical properties. The FS/CS ratio was found to be predicted within the range of 0.11-0.20 and the STS/CS ratio was found between 0.07 to 0.11. The ratios observed was very close to the experimental values too. These intervals are consistent with known mechanical behavior of cementitious composites, and refer to the fact that the model maintains realistic proportionate relationships

among various strengths parameters. The capacity to concurrently forecast various properties and yet retain the physical interdependence of the properties, are further indicators of the high degree of generalization and predictive stability of the GB model. From the point of view of models' applicability limits, the model performs reliably within the range of input values seen during training. For the GB-tuned model, the valid ranges are: GGBS: 0–338.18 kg/m^3, SMS: 0–59.18 kg/m^3, CH: 0–33.81 kg/m^3, CC: 0–422.72 kg/m^3, NFA: 591.66–625.62 kg/m^3, NCA: 1175.7–1230.3 kg/m^3, w/b ratio: 0.44–0.55, and curing time: 3–28 days. Within these limits, the model provides reliale and consistent predictions, while inputs outside these ranges or unseen combinations resultsed in less reliable results, this is because of the fact that the model was not designed to extrapolate beyond its training data.

In conclusion, GB model showed excellent accuracy, reliability and strength simultaneously predicting CS, FS, and STS. The large socres of R^2, the small amounts of the prediction errors, and the evenly distributed values clearly demonstrate that the model has the capability of representing the intricate nonlinear inter-relationships among mix-design variables and mechanical properties. In addition, GB maintains realistic strength ratios, and it is also equally efficient in OPAAC and traditional concrete mixes. Although GB was the best-performing model, the RF model demonstrated high predictive rates as well and took the second place. These outcomes were in line with the prior studies, which details the effectiveness of ensemble techniques, as indicated by Harika et al. [44], they found RF to be the best model when predicting CS in a one-part AAB mortar than GB and decision tree with SVR coming after. Arun et al. [37] reported that the GB model was the best in prediction of CS for geopolymer concrete developed in their work. Hence, the current findings demonstrate the usefulness, flexibility, and stability of ensemble ML methods to provide precise multi-strength predictions of OPAAC in research and practice

3.4. Environmental and Economic Aspects

The benefits in terms of environment were determined by finding the carbon emission value regarding raw materials used in the mix compositions. The carbon emissions factors, in kg CO_2-eq per kg of material, were taken from existing sources of literature [17,46,53] and are presented in Table 10. The calculation was restricted to the material production phase of concrete using the formulated mix design, and did not consider the transportation, construction, service life, and end-of-life phases. This allows for a direct comparison between OPAAC and CC concrete, which is already available in the market and well-known for its lower embodied carbon content ~44-47% lesser than that of conventional 100% OPC-based concrete. This is necessary to point that such significant cut of carbon emissions is supported with relatively small economic benefits since CC is usually offered at a lower price than OPC, thus making it a viable low-carbon option. The quantity of total emissions per cubic meter (kg CO_2-eq/m^3) was calculated as the product of the quantity of each component (Table 5) and its emission factor (Table 10). The calculations (Figure 12a) suggested that OPAAC mixes result in an additional 20-22% embodied-carbon saving compared to CC concrete mixes. In case of same mix ratios of OPC (emission factor ~ 0.85 kg CO_2-eq/kg), when OPC is used as a binder rather than CC, the overall carbon emissions of the OPC-based concrete mixes (M15, M20, and M25) were estimated to be 380.25, 419.50, and 447.68 kg/m^3 of concrete respectively. When comparing the outcomes obtained using OPC-based conventional concrete, it is possible to note that the implementation of OPAAC leads to the general decrease in carbon emissions by 55-59%.

A parallel analysis was also done on the costs of ingredients of the concrete mixes formulated. The unit cost of the materials (Table 10) was chosen based on the prevailing market prices in India and estimates as given in the previous research works [11,46,54]. Despite the fact that the cost of materials may change depending on the supplier, geographical location, distance of transportation, and quantity of purchase, the chosen costs are average market prices appropriate for comparative purposes. The total cost per m^3 of the concrete was calculated by multiplying amounts of materials in Table 5 by their unit costs in Table 10. Figure 12b shows the total unit volume cost of each mix grade and type of binder. OPAAC mixes showed a cost-saving potential of about 10–13% in comparison to the use of CC concrete. Using the same mix ratios, the OPC (Unit cost ≈ 0.0861 $/kg) as the binder rather than the CC, the estimated cost of the OPC-based concrete of M15, M20, and

M25 mixes were 44.12, 47.91, and 50.70 $/kg per m^3 of concrete, respectively. When compared to OPC-based conventional concrete, OPAAC leads to the overall reduction in cost by about 12-16%. In a practical perspective, the carbon-emission reduction along with the cost-saving consideration highlights the massive potential of OPAAC mixes as an economically feasible and environmentally friendly alternative to ordinary or even a standard grade of concrete.

Table 10. Emission factor and unit cost of ingredients of concrete

Material	Emission factor (kg CO_2-eq/kg)	Cost rate* ($/kg)
CC	0.35	0.0828
GGBS	0.07	0.0243
SMS	0.80	0.3091
CH	0.94	0.1325
NFA	0.05	0.0055
NCA	0.05	0.0094
Water	0.00	0.0000

**Cost of ingredients as per Indian scenario converted from INR to US$ [1 US$ ~ 90.60 INR (₹) in Feb 2026].*

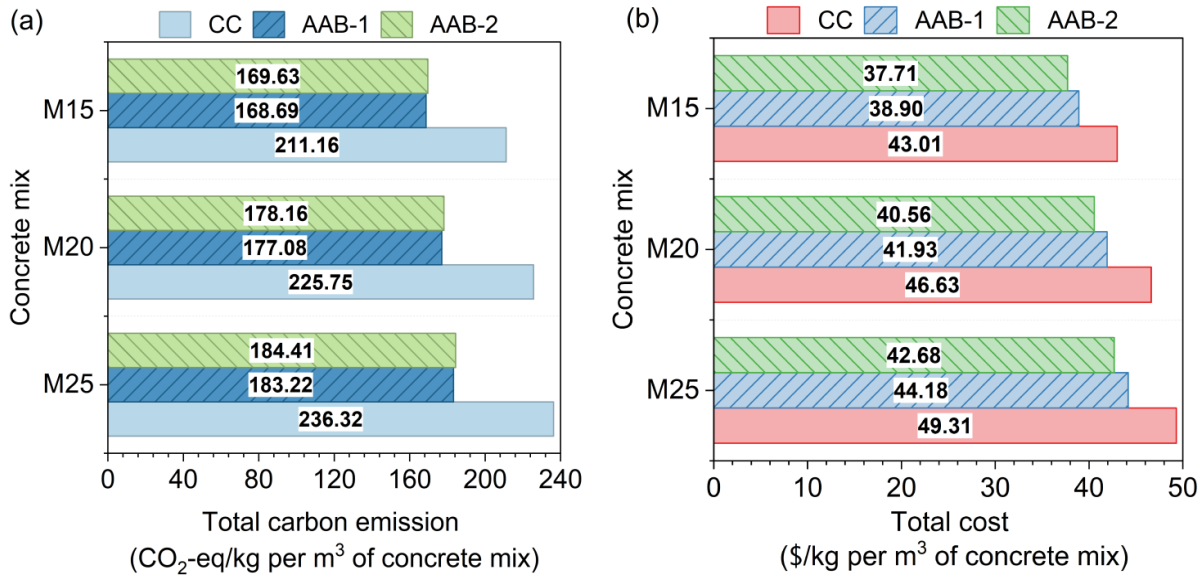

Fig. 12. Carbon emissions and total cost of developed concrete mixes

3.5. Comparison with Recent OPAAC Studies

Table 11 reveals the latest researches on one-part alkali-activated/ geopolymer concrete (OPAAC) that uses solid precursors, powder alkali activators, natural aggregates, water and superplasticizer. The review of these studies reveals that the most common solid precursor in OPAAC was either GGBS or a binary mixture of FA and GGBS.

The most widespread activators were the silicate-based activators that could be utilized individually or could be combined with both additional activators to control the system alkalinity and silica modulus. This has been widely used to enhance rapid reaction and enhance early development of strength. The comparative analysis further indicates that most of the previous studies have mainly been concerned with achieving the high to ultra-high CS by means of optimization of mix design parameters, such as precursor composition, quantity of the activators, w/b ratio, and curing methods. Mostly employed curing regimes were ambient and water curing, which highlights the increasing importance of focusing on the OPAAC systems that can be as efficient without the usage of high-temperature treatment. These studies also suggested that the workability of OPAAC can be improved as per the requirement by utilizing superplasticizers.

Table 11. Performance comparison of OPAAC developed in recent studies

One-part Binder (B)		Aggregate	Mix grade/ ratio (B:NFA:NCA)	Curing Method	Strength of concrete at 28 d (MPa)			Ref.
Precursor	Activator				CS	FS	STS	
GGBS	SHMP	NCA, NFA	1:1.59:2.83 W/B-0.45	Ambient	33.48	4.27	2.31	[32]
GGBS	SHMP	NCA, NFA	1:1.59:2.83 W/B-0.45	Water	32.00	4.53	2.38	[32]
FA, GGBS	K_2CO_3	NCA, NFA	1:1.48:2.84, W/B-0.3, SP- 1.4% wt of B	Ambient	11.40	-	-	[55]
FA, GGBS	SS, Na_2CO_3	NCA, NFA	M40	Ambient	47.50	6.30	4.60	[33]
FA, GGBS	SS, Na_2CO_3	NCA, NFA	M50	Ambient	61.00	7.10	5.10	[33]
GGBS	SMS Pentahydrate	NCA, NFA	SMS/GGBS-0.16, NFA/GGBS-2.26, NCA/NFA-0.66, W/GGBS-0.45	Water	56.11	6.54	3.33	[21]
GGBS	SMS anhydrous	NCA, NFA	M30	Water	36.24	-	-	[34]
GGBS	SMS anhydrous	NCA, NFA	M50	Water	55.28	-	-	[34]
FA, GGBS	SMS anhydrous	NCA, NFA	M40	Ambient	51.60	-	-	[31]
FA, GGBS	Crystalline hydrated sodium silicate	NCA, NFA	M30–M50	Ambient	30.40 to 47.10	3.60 to 5.40	3.34 to 4.70	[29]
FA, GGBS	SMS Anhydrous	NCA, NFA	FA/GGBS-0.33, SMS/GGBS-0.18, W/FA+GGBS-0.4, NFA/FA+GGBS-0.86, NCA/NFA-0.85, SP-1.3% (FA+GGBS)	Ambient	76.70	7.20	~4.6	[56]
GGBS	SMS Anhydrous	NCA, NFA	GGBS:NFA:NCA-1:2.2:4 SMS/GGBS-0.163, W/B-0.41 SP/GGBS-0.02	Ambient	47.97	~4.7	4.80	[11]
FA	SMS Pentahydrate, NaOH (16M)	NCA, NFA	NFA/FA-0.84 NCA/FA-1.93 SMS/FA-0.093 NaOH/FA-0.09 W/FA-0.22	Ambient	68.60	-	6.10	[57]
FA, GGBS	SMS Anhydrous	NCA, NFA	1:1.42:2.72 W/B-0.344 SP/B-0.016	Ambient	37.10	-	-	[13]
GGBS	SMS anhydrous, $Ca(OH)_2$	NCA, NFA	M15 (1:1.85:3.64) W/B-0.55	Water	22.38	4.02	2.28	Current study
GGBS	SMS anhydrous, $Ca(OH)_2$	NCA, NFA	M20 (1:1.58:3.07) W/B-0.48	Water	27.88	5.08	2.86	Current study
GGBS	SMS anhydrous, $Ca(OH)_2$	NCA, NFA	M25 (1:1.40:2.78) W/B-0.44	Water	32.72	6.20	3.44	Current study

Notations:- B= (Precursor + Activator), SMS-Sodium Metasilicate, SHMP-Sodium Hexametaphosphate, SS-Sodium Silicate, FA-Fly Ash, NFA-Natural Fine Aggregate, NCA-Natural Coarse Aggregate, W/B- Water to Binder Ratio, SP- Superplasticizer

The CS in the current study was relatively lower as compared to those established in some high-performance OPAAC systems [11,21,29,31,33,34,56,57], but was similar to some moderate-strength mixtures [13,32,34]. It is necessary to mention that the aim of this research was not to make the maximum CS but to create structurally viable mixes to be used in the practical applications in the low- to medium-strength concrete. Interestingly, the CS that was achieved was lower, but the tensile strength values were similar to those in other literature. The behavior can be attributed to the phenomenon that alkali-activated paste leads to stronger interfacial bonding with aggregates and this leads to higher tensile performance and resistance to cracks. The mix proportioning in the current study was done through the conventional Indian Standard mix design method (IS 10262:2019 [49]), that is used in OPC concrete, unlike most of the earlier studies which had used tailored or experimentally optimized mix design methodologies that was unique to alkali-activated systems. However, few studies [11,32] developed OPAAC with similar Indian Standard mix design method in their studies earlier. In current study, the alkali -activated binders (AAB-1 and AAB-2) were considered to be equivalent to OPC 33-grade in terms of physical properties and mix design procedure was carried out in a similar way as conventional concrete. This was deliberately selected as a way of testing the viability of implementing OPAAC into the current construction operations without the need to make significant changes to the current design procedures. The CS goals were restricted to the following grades- M15, M20, and M25; developed without using any chemical admixture. This was a practical decision, since a large percentage of the current construction activity within the local environment, especially residential construction, rigid pavements, and general-purpose structural constructions, needs concrete grades of no more than M25. As such, this research lays focus on applicability, constructability, and adaptability in the current construction requirements, and does not only consider high-strength performance. This kind of strategy promotes the possibility of implementing OPAAC at the field level since it is an environmentally friendly and user-friendly substitute to conventional concrete.

4. Conclusions

The current study determined the fresh workability and hardened strength for OPAAC of M15, M20 and M25 grades and determined predictive modeling by applying machine-learning processes. On the basis of the experimental and analytical studies, the following conclusions are made:

- Workability of OPAAC increased as proportions of sodium metasilicate and calcium hydroxide increased, and further increase of the workability was detected with high levels of w/b ratios. The slump values of OPAAC mixes were equivalent to the control mix.
- OPAAC has a relatively higher mechanical strength compared to conventional concrete. Among the mixes, AAB-1 concrete had the best results in compressive, flexural, and split tensile tests when compared to its control mix and AAB- 2. In particular, the CS ranges between 22.38-32.72 MPa, FS between 4.02-6.20 MPa and STS between 2.28-3.44 MPa, thus, indicating that OPAAC can provide similar strength to that of conventional concrete in terms of field construction requirements.
- Ensemble-based ML models, such as gradient boosting (GB) and random forest (RF), were effective in multi-strength prediction of OPAAC. The GB model was able to predict CS, FS and STS at the same time with R^2 scores of 0.9679, 0.9716 and 0.9656, respectively, with low magnitudes of RMSE and MAE. Overall GB model exhibited an average R^2 of 0.9684 with very low errors.
- The environmental and economic benefits of OPAAC with 55-59 % lesser carbon emissions and cost savings of 12-16 %, which validates the idea that the material can serve as a low-carbon and low-cost binder.

Overall, the developed OPAAC is offering similar levels of workability, better mechanical performance, significant carbon savings, cost-saving, and predictable mechanical performance through machine-learning. It also defeats the limitations of liquid activators within a two-part system, allowing conventional mix-design solutions, as well as increasing field applicability. All of these benefits make OPAAC a feasible and viable alternative to traditional concrete in field construction works. Even though the results are promising, the current study is limited to small range of strength grades, particular material mixtures, and laboratory-level performance checks.

Future research may investigate formulation of the high strength concrete mix design, usage of chemical admixtures, durability assessment, microstructural evaluations, application of ML models on larger dataset, and the full life cycle assessment. These efforts may enhance the credence in the performance, durability and the widespread applicability of OPAAC in large construction works.

References

[1] GCCA United Kingdom. Concrete Future – Roadmap to Net Zero. Global Cement and Concrete Association; 2021. Accessed February 12, 2026. Available from: https://gccassociation.org/concretefuture/wp-content/uploads/2022/10/GCCA-Concrete-Future-Roadmap-Document-AW-2022.pdf

[2] Nejad BM, Enferadi S, Andrew R. A comprehensive analysis of process-related CO2 emissions from Iran's cement industry. Cleaner Environmental Systems. 2025;16:100251. https://doi.org/10.1016/j.cesys.2024.100251.

[3] Karadumpa CS, Pancharathi RK. Study on energy use and carbon emission from manufacturing of OPC and blended cements in India. Environ Sci Pollut Res. 2024;31:5364–5383. https://doi.org/10.1007/s11356-023-31593-3.

[4] Bureau of Indian Standards. IS 16415: 2015 Composite Cement-Specification. New Delhi: BIS; 2015.

[5] Lanjewar BA, Chippagiri R, Dakwale VA, Ralegaonkar RV. Application of Alkali-Activated Sustainable Materials: A Step towards Net Zero Binder. Energies. 2023;16(2):969. https://doi.org/10.3390/en16020969.

[6] Meshram RB, Kumar S. Comparative life cycle assessment (LCA) of geopolymer cement manufacturing with Portland cement in Indian context. Int J Environ Sci Technol. 2022;19:4791–4802. https://doi.org/10.1007/s13362-021-03336-9.

[7] Aiken TA, Gu L, Kwasny J, Huseien GF, McPolin D, Sha W. Acid resistance of alkali-activated binders: A review of performance, mechanisms of deterioration and testing procedures. Constr Build Mater. 2022;342:128057. https://doi.org/10.1016/j.conbuildmat.2022.128057.

[8] Mohamed OA. A Review of Durability and Strength Characteristics of Alkali-Activated Slag Concrete. Materials. 2019;12(8):1198. https://doi.org/10.3390/ma12081198.

[9] Mahendra K, Narasimhan MC. One part alkali-activated materials for construction – A review. Mater Today Proc. 2023;93:182–188. https://doi.org/10.1016/j.matpr.2023.07.116.

[10] Luukkonen T, Sreenivasan H, Abdollahnejad Z, Yliniemi J, Kantola A, Telkki VV, et al. Influence of sodium silicate powder silica modulus for mechanical and chemical properties of dry-mix alkali-activated slag mortar. Constr Build Mater. 2020;233:117354. https://doi.org/10.1016/j.conbuildmat.2019.117354.

[11] Yankesh, Pal R, Singh N, Priyadarshee A, Rana D, Kumar V. Performance Evaluation of One-Part Geo-Polymer Concrete. Procedia Struct Integrity. 2025;70:311–318. https://doi.org/10.1016/j.prostr.2025.07.058.

[12] Rostami M, Nasrollahzadeh K, Zwicky D. Durability of alkali-activated slag concrete with sodium metasilicate powder as activator under nitric acid attack. Adv Cem Res. 2025:1–13. https://doi.org/10.1680/jadcr.24.00227.

[13] Jahandari S, Tao Z, Rahmani A, Alim MA. Durability of one-part geopolymer concrete in aggressive environments. Constr Build Mater. 2025;490:142510. https://doi.org/10.1016/j.conbuildmat.2025.142510.

[14] Kumar A, Kumar V, Prasad B. Strength development and flexural behavior of reinforced concrete beam using one-part alkali-activated binder. Constr Build Mater. 2021;281:122619. https://doi.org/10.1016/j.conbuildmat.2021.122619.

[15] Reddy RRK, Yaragal SC, Srinivasa AS. One-part eco-friendly alkali-activated concrete–An innovative sustainable alternative. Constr Build Mater. 2023;408:133741. https://doi.org/10.1016/j.conbuildmat.2023.133741.

[16] Ghafoor MT, Rakhimova N, Shi C. One part geopolymers: A comprehensive review of advances and key challenges. J Build Eng. 2025;111:113112. https://doi.org/10.1016/j.jobe.2025.113112.

[17] Rashid K, Raoof MN, Daud M, Wang Y, Ju M. One-part alkali activated binder activated by sodium metasilicate and ternary-factored sustainability of structural block. Structures. 2024;68:107108. https://doi.org/10.1016/j.istruc.2024.107108.

[18] Alhamoud A, Riahi HT, Ataei A. Mechanical properties and stress-strain relationship of slag-based one-part geopolymer concrete: A comparative study. Results Eng. 2024;24:102952. https://doi.org/10.1016/j.rineng.2024.102952.

[19] Ren J, Sun H, Li Q, Li Z, Ling L, Zhang X, et al. Experimental comparisons between one-part and normal (two-part) alkali-activated slag binders. Constr Build Mater. 2021;309:125177. https://doi.org/10.1016/j.conbuildmat.2021.125177.

[20] Oderji SY, Chen B, Ahmad MR, Shah SFA. Fresh and hardened properties of one-part fly ash-based geopolymer binders cured at room temperature: Effect of slag and alkali activators. J Clean Prod. 2019;225:1–10. https://doi.org/10.1016/j.jclepro.2019.03.290.
[21] Abdulkarim A, Riahi HT, Ataei A. Comparative study of mechanical properties of one-part alkali-activated slag concrete using deformed and recycled tire steel fibers. Case Stud Constr Mater. 2025;22:e04124. https://doi.org/10.1016/j.cscm.2024.e04124.
[22] Ma C, Long G, Shi Y, Xie Y. Preparation of cleaner one-part geopolymer by investigating different types of commercial sodium metasilicate in China. J Clean Prod. 2018;201:636–647. https://doi.org/10.1016/j.jclepro.2018.08.060.
[23] Oderji SY, Chen B, Ahmad MR, Shah SFA. Fresh and hardened properties of one-part fly ash-based geopolymer binders cured at room temperature: Effect of slag and alkali activators. J Clean Prod. 2019;225:1–10. https://doi.org/10.1016/j.jclepro.2019.03.290.
[24] Ouyang S, Chen W, Zhang Z, Li X, Zhu W. Experimental study of one-part geopolymer using different alkali sources. J Phys Conf Ser. 2020;1605:012155. https://doi.org/10.1088/1742-6596/1605/1/012155.
[25] Alrefaei Y, Wang YS, Dai JG, Xu QF. Effect of superplasticizers on properties of one-part Ca(OH)2/Na2SO4 activated geopolymer pastes. Constr Build Mater. 2020;241:117990. https://doi.org/10.1016/j.conbuildmat.2019.117990.
[26] Askarian M, Tao Z, Samali B, Adam G, Shuaibu R. Mix composition and characterisation of one-part geopolymers with different activators. Constr Build Mater. 2019;225:526–537. https://doi.org/10.1016/j.conbuildmat.2019.07.083.
[27] Gao H, Al-Damad IMA, Siddika A, Kim T, Foster S, Hajimohammadi A. Enhancing the workability retention of one-part alkali activated binders by adjusting the chemistry of the activators. Cem Concr Compos. 2025;157:105928. https://doi.org/10.1016/j.cemconcomp.2025.105928.
[28] Ali N, Soliman AM. Influence of mixing protocols on flow retention of one-part alkali activated slag systems. Constr Build Mater. 2024;450:138467. https://doi.org/10.1016/j.conbuildmat.2024.138467.
[29] Pham TT, Nguyen NL, Nguyen TT, Nguyen TT, Pham TH. Effects of Superplasticizer and Water–Binder Ratio on Mechanical Properties of One-Part Alkali-Activated Geopolymer Concrete. Buildings. 2023;13(7):1835. https://doi.org/10.3390/buildings13071835.
[30] Haruna S, Mohammed BS, Wahab MMA, Liew MS. Effect of paste aggregate ratio and curing methods on the performance of one-part alkali-activated concrete. Constr Build Mater. 2020;261:120024. https://doi.org/10.1016/j.conbuildmat.2020.120024.
[31] Sun D, Lee J, Mohyeddin A, Migunthanna J. Mechanical Properties and Reproducibility of One-Part Ambient-Cured Slag and Fly Ash-Based Geopolymer Concrete. Buildings. 2026;16(4):707. https://doi.org/10.3390/buildings16040707.
[32] Kumar V, Kumar A, Prasad B. Mechanical behavior of non-silicate based alkali-activated ground granulated blast furnace slag. Constr Build Mater. 2019;198:494–500. https://doi.org/10.1016/j.conbuildmat.2018.11.282.
[33] Neupane K. Evaluation of environmental sustainability of one-part geopolymer binder concrete. Cleaner Materials. 2022;6:100138. https://doi.org/10.1016/j.clema.2022.100138.
[34] Sharma D, Singh RB. Strength-based design mix methodology of one-part geopolymer concrete using response surface methodology. Multiscale Multidiscip Model Exp Des. 2025;8:120. https://doi.org/10.1007/s41939-024-00713-y.
[35] Mahendra K, Narasimhan MC, Rathod S, Das AK, Prakash GB. Durability performance of one-part alkali-activated self-compacting concrete mixes under aggressive and elevated temperature conditions. Sustain Chem Pharm. 2025;45:102025. https://doi.org/10.1016/j.scp.2025.102025.
[36] Karabaş C, Niş A. Durability of Alkali-Activated Concretes Under 5% Sulfuric Acid Environment. J Sustain Constr Mater Technol. 2025;10. https://doi.org/10.29187/2458-973X.1203.
[37] Arun BR, Srishaila JM, S MK, Algur V, K K, Tanu H. Prediction of machine learning application in the development of novel sustainable self-compacting geopolymer concrete. Res Eng Struct Mater. 2024. https://doi.org/10.17515/resm2024.354ma0716rs.
[38] Mahajan L, Bhagat S. Machine learning approaches for predicting compressive strength of concrete with fly ash admixture. Res Eng Struct Mater. 2023;9(2):431–456. https://doi.org/10.17515/resm2022.534ma0927.
[39] Hasan MM, Xu J, Uddin MN, Yang J, Tonny NJ. An interpretable machine learning approach to predict the compressive strength of fly ash-based geopolymer concrete. Innov Infrastruct Solut. 2025;10:500. https://doi.org/10.1007/s41062-025-02307-0.
[40] Khan AQ, Naveed MH, Rasheed MD, Miao P. Prediction of Compressive Strength of Fly Ash-Based Geopolymer Concrete Using Supervised Machine Learning Methods. Arab J Sci Eng. 2024;49:4889–4904. https://doi.org/10.1007/s13369-023-08283-w.

[41] Huseien GF, Baghban MH, Faridmehr I, Dong K. Optimizing Mix Design for Alkali-Activated Concrete: A Comprehensive Review of Critical Selection Factors. CivilEng. 2025;6(3):43. https://doi.org/10.3390/civileng6030043.
[42] Fareghian M, Afrazi M, Armaghani DJ, Akhoundan M, Asghari N, Yazdani M. Machine Learning in the Modeling of 3D Printed Soil-Cement Materials: A Short Overview. J Soft Comput Civil Eng. 2026;10. https://doi.org/10.22115/scce.2025.1966.
[43] Afrazi M, Armaghani DJ, Afrazi H, Fattahi H, Samui P. Real-time monitoring of tunnel structures using digital twin and artificial intelligence: A short overview. Deep Undergr Sci Eng. 2025:1–16. https://doi.org/10.1002/dug2.70029.
[44] Harika R, Venkateswara Rao S, Ramujee K, Keerthan B. Analytical and experimental investigation on strength characteristics of one part geopolymer using machine learning models. Asian J Civ Eng. 2025. https://doi.org/10.1007/s42107-025-01602-6.
[45] Abdel-Mongy M, Iqbal M, Farag M, Yosri AM, Alsharari F, Yousef SEAS. Artificial Intelligence Prediction of One-Part Geopolymer Compressive Strength for Sustainable Concrete. CMES. 2024;141:525–543. https://doi.org/10.32604/cmes.2024.052505.
[46] Kumar S, Sinha AK. Development of eco-friendly concrete paving blocks utilizing one-part alkali-activated binders. Res Eng Struct Mater. 2026;12. https://doi.org/10.17515/resm2025-963ma0612rs.
[47] Bureau of Indian Standards. IS 383-2016 (Reaffirmed 2021) Coarse and Fine Aggregate for Concrete Specification (Third Revision). New Delhi: BIS; 2016.
[48] Bureau of Indian Standards. IS 456: 2000 (Reaffirmed 2021) Plain and Reinforced Concrete Code of Practice (Fourth Revision). New Delhi: BIS; 2000.
[49] Bureau of Indian Standards. IS 10262: 2019 Concrete Mix Proportioning Guidelines (Second Revision). New Delhi: BIS; 2019.
[50] Bureau of Indian Standards. IS 1199 (Part 2): 2018 Fresh Concrete - Methods of Sampling, Testing and Analysis Part 2 Determination of Consistency of Fresh Concrete (First Revision). New Delhi: BIS; 2018.
[51] Bureau of Indian Standards. IS 516 (Part 1/Sec 1): 2021 Hardened Concrete Methods of Test Part 1 Testing of Strength of Hardened Concrete Section 1 Compressive, Flexural and Split Tensile Strength (First Revision). New Delhi: BIS; 2021.
[52] ACI Committee 318. Building code requirements for structural concrete (ACI 318-05) and commentary (ACI 318R-05). Farmington Hills, MI: American Concrete Institute; 2005.
[53] Jameel M, Suteerasak T, Chumpol P, Puttiwongrak A, Sae-Long W, Sukontasukkul P. Properties of one-part geopolymer pedestrian blocks made using 100 % waste materials. Case Stud Constr Mater. 2025;22:e04538. https://doi.org/10.1016/j.cscm.2025.e04538.
[54] Sengupta J, Dhang N, Deb A. Life cycle sustainability assessment of one-part alkali-activated concrete activated with industrial grade soda ash and hydrated lime-A comparative study. Sustain Chem Pharm. 2025;48. https://doi.org/10.1016/j.scp.2025.102254.
[55] Askarian M, Tao Z, Adam G, Samali B. Mechanical properties of ambient cured one-part hybrid OPC-geopolymer concrete. Constr Build Mater. 2018;186:330–337. https://doi.org/10.1016/j.conbuildmat.2018.07.160.
[56] Mahendra K, Narasimhan MC, Prakash GB, Das AK. Experimental investigation and optimization of one-part alkali-activated self-compacting concrete mixes. Case Stud Constr Mater. 2024;21:e04062. https://doi.org/10.1016/j.cscm.2024.e04062.
[57] Wibowo YN, Piscesa B, Tajunnisa Y, Sutrisno W. Investigation on the mechanical behavior of high-calcium fly ash geopolymer concrete using one-part method. Constr Build Mater. 2025;490:142436. https://doi.org/10.1016/j.conbuildmat.2025.142436.